ELASTIC LATERAL BUCKLING LOAD OF CONTINUOUS BRACED H-SHAPED BEAMS WITH FORK RESTRAINT UNDER GRADIENT BENDING MOMENTS

YUI SATO[1,2], YUKI YOSHINO[3] & YOSHIHIRO KIMURA[2]
[1]JFE Civil Engineering and Construction Corp., Japan
[2]Tohoku University, Japan
[3]National Institute of Technology Sendai College, Japan

ABSTRACT

In Japan, medium- and low-rise steel structures predominantly consist of moment frames with H-beams connected to box columns. The high torsional rigidity of these columns effectively constrains lateral buckling deformations induced by seismic bending moments in the beams. Previous studies have demonstrated that when H-beams are connected to box columns, flange warping and out-of-plane deformation at the beam ends are restricted, approaching fully fixed support. In this paper, warping fixed support is assumed for the boundary condition of beam ends, and the additional restraint necessary for fully fixed support is defined as fork restraint. Japanese steel structure design guidelines assume pinned beam ends when calculating lateral buckling loads and plastic deformation capacity. However, beam ends typically exhibit fork restraint in practice. Additionally, non-structural members, such as roof folded plates, are attached to the beams and continuously constrain lateral buckling deformations along the beam's length. This paper examines the effect of boundary conditions on the elastic lateral buckling load of continuously braced H-beams under antisymmetric bending moments. First, the elastic lateral buckling load is calculated for beams with warping and fully fixed supports using the energy method. The resulting equations are then applied to beams with fork restraint, due to the columns' torsional resistance. A numerical analysis is performed, modelling the H-beam with four-node shell elements and continuous braces represented by horizontal and rotational springs. The proposed equations are validated by comparison with numerical analysis results. The findings show that the elastic lateral buckling load increases with greater horizontal and rotational rigidity of continuous braces and enhanced fork restraint at the beam ends. The load also improves when the bending moment distribution approaches an antisymmetric pattern. The proposed equation provides a practical method to evaluate the lateral buckling load of continuously braced H-beams with fork restraint.

Keywords: lateral buckling, fork restraint, continuous brace, gradient bending moments.

1 INTRODUCTION

In Japan, medium- and low-rise steel buildings primarily utilize moment-resisting frames, with H-beams rigidly connected to box columns, as shown in Fig. 1. The high torsional rigidity of these columns reduces lateral buckling of beams during earthquakes. However, Japanese design guidelines assume that beam ends are pinned for lateral buckling load and plastic deformation capacity calculations.

A previous study [1] has shown that connecting H-beams to box columns constrains flange warping at the beam ends, creating nearly warping fixed support and restraining fork deformation, which is lateral bending deformation of beam end flanges in the axial direction, as shown in Fig. 1. This study defines fork restraint as boundary conditions from warping-fixed to fully fixed support.

Large-span beams are prone to torsion in the weak axis direction, and when lateral buckling occurs, the beam cannot achieve its full plastic strength. Therefore, braces are required to prevent lateral buckling of the beam. A previous study [2] has shown that even non-structural members such as roof folded plates can also restrain lateral buckling

WIT Transactions on The Built Environment, Vol 217, © 2025 WIT Press
www.witpress.com, ISSN 1743-3509 (on-line)
doi:10.2495/ERES250091

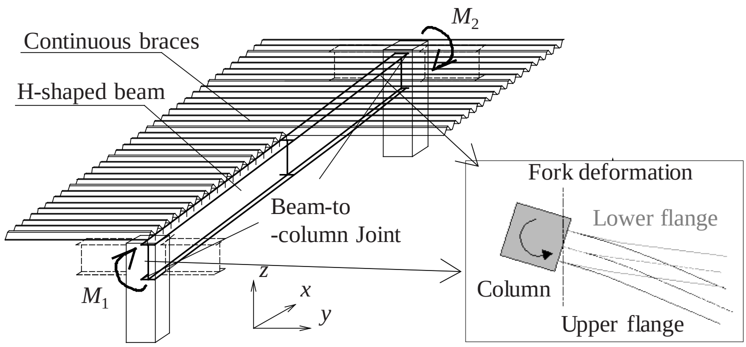

Figure 1: Continuous braced H-shaped beam and fork deformation.

deformation when attached continuously along the beam's length. Kimura and Sato [1] elucidated the influence of boundary conditions on the elastic lateral buckling load of continuously braced H-beams under uniform bending moments.

In this study, the following aspects are examined for beams subjected to gradient bending moments. The energy method is used to derive the elastic lateral buckling load equation for H-beams under gradient moments with fully fixed support. In Kimura and Sato [1], the lateral buckling load equation for warping-fixed support is deduced. Therefore, the elastic lateral buckling load equation for the case of restrained fork deformation, which falls between warping-fixed support and fully fixed support, is obtained using the ratio of fork rigidity. Finally, comparing numerical analysis with the buckling load equation reveals the relationship among fork restraint, moment gradient, and buckling load.

2 TARGET CROSS SECTION AND NUMERICAL ANALYSIS MODEL

In this study, the slenderness ratio is denoted as λ_1, defined by eqn (1). The range of λ_1 considered is 160 to 280.

$$\lambda_1 = \frac{l}{i_1}., \quad i_1 = \sqrt{\frac{I_f}{A_1}} \quad A_1 = A_f + \frac{A_w}{6}. \tag{1}$$

where A_1 represents the effective cross-sectional area under compressive force when the bending moment at the H-beam end is converted to a uniform force. The H-beam cross sections covered in this paper are H-500×250×9×16, H-600×200×11×17, and H-390×300×10×16.

Next, the fork restraint at the beam ends covered in this paper is explained. Fig. 2 shows the relationship between the fork rigidity $\overline{K}_f$ at the beam ends and the column-to-beam capacity ratio M_{pc}/M_{pb}. $\overline{K}_f$ is derived from eqn (2):

$$\overline{K}_f = M_T/\phi = GK_c/2h. \tag{2}$$

where M_T: bending torsional moment due to fork deformation of the beam, ϕ: rotation angle of the web caused by fork deformation, GK_c: St Venant torsional rigidity due to column torsional resistance, h: story height. The column cross-sections are typical box and H-beam sections used in Japan [3], with heights ranging from 3 to 5 m. Assuming M_{pc}/M_{pb} between 1.3 and 2.0, the fork rigidity at beam ends is $\log(\overline{K}_f)$ = 2.0 to 5.4.

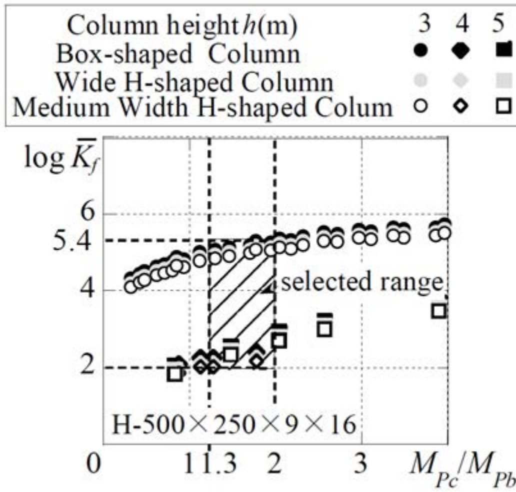

Figure 2: Relationship between column-to-beam's rotational rigidity and strength ratio.

Given that beams are generally attached in four directions at column ends, the lower limit of fork rigidity is approximately $25 \approx 10^{1.4}$, which is 1/4 of $\overline{K}_f$=100 (log($\overline{K}_f$) = 2.0). Thus, the range of log($\overline{K}_f$) considered in this study is 1.4 to 5.4.

The loading conditions for H-beams are outlined as follows. In this study, the bending moments at the beam ends are replaced by axial forces acting on the upper and lower flanges, denoted as P_{11}, P_{12}, P_{21}, and P_{22} in Fig. 3.

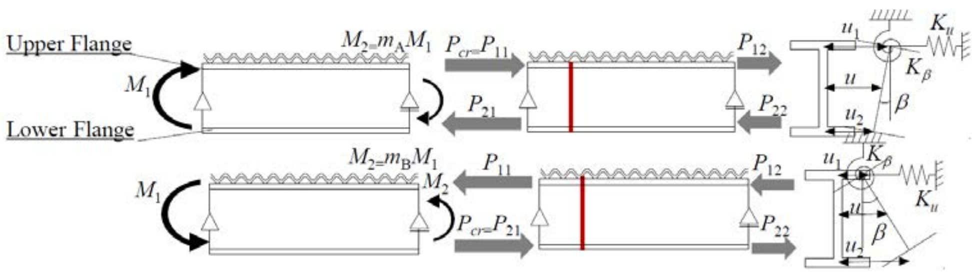

Figure 3: Loading conditions.

It is assumed that the bending moment M_1 at the left end is consistently greater than the bending moment M_2 at the right end, with m_k ranging from −1 to 1. Here, m_k = −1 represents a flexural bending moment, while m_k = 1 signifies an antisymmetric bending moment. The right subscript k = N indicates the moment slope without bracing and A or B indicates the moment slope when the H-beam is braced. Also, for k=A, the load condition is Type A. For k = B, the load condition is Type B. The loading conditions are explained below. The braces are attached to the upper flange, defining it as the upper flange, while the flange without braces is the lower flange. For beams under gradient bending moments, Type A is dominated by compressive stress on the upper flange due to M_1, and Type B is dominated by compressive stress on the lower flange due to M_1.

This study employs the horizontal rigidity ratio $K_u/(EI_f/l^3)$, which compares the horizontal rigidity of the bracing material to the bending rigidity of the H-beam, and the rotational rigidity ratio $K_\beta/(GK_f/d)$, which compares the rotational rigidity of the bracing material to the torsional rigidity of the H-beam, as indicators of rigidity. Here, I_f: the sectional moment of inertia of the upper or lower flange about the beam's weak axis, G: the beam's elastic shear modulus, K_f: the flange's torsional constant, l: the beam length, and d: the distance between the centres of the upper and lower flanges. K_u (kN/mm) represents horizontal rigidity, and K_β (kN mm/rad) represents rotational rigidity. The required rigidity ratio is the combination of these ratios when the buckling mode shifts from 1st order to 2nd order under warping-fixed support and uniform bending moment.

Fig. 4 shows the required rigidity ratio curve for H-500×250×9×16 with λ_1 = 200. The grey line represents Type A, and the black line represents Type B. On the required rigidity ratio curve in Type B, $K_u/(EI_f/l^3)$ at $K_\beta/(GK_f/d) = \infty$ is $k_{u,min}$, and $K_\beta/(GK_f/d)$ at $K_u/(EI_f/l^3) = \infty$ is $k_{\beta,min}$. These coordinates, $K_{min}(k_{u,min},\ k_{\beta,min})$, marked by ○, serve as indicators for setting the reference required rigidity ratio. The intersection points of lines through the origin and K_{min} with the rigidity ratio curves for Type A and Type B are the reference required rigidity ratios ${}_AK_0({}_Ak_{u0},\ {}_Ak_{\beta0})$ and ${}_BK_0$ $({}_Bk_{u0},\ {}_Bk_{\beta0})$ (□, ■ in the figure). The ratio of arbitrary rigidity to ${}_kK_0$ will be used as a parameter, where the subscript k denotes A for Type A and B for Type B.

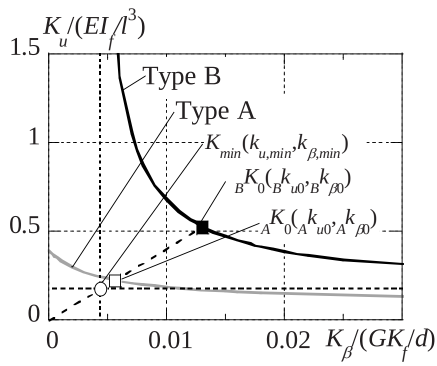

Figure 4: Relationship between horizontal rigidity ratio and rotational rigidity ratio.

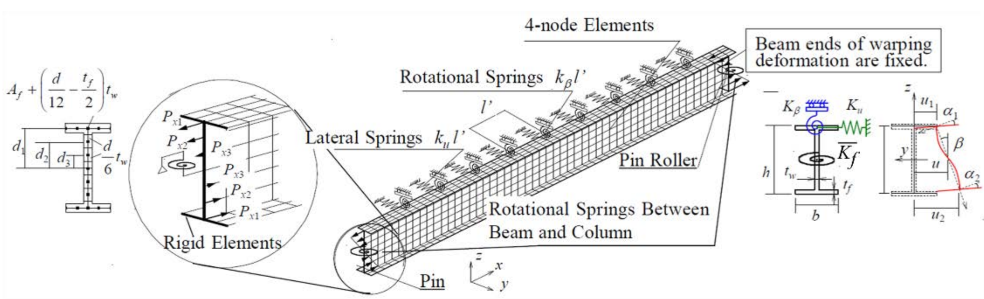

Figure 5: Numerical analysis model.

Fig. 5 depicts the numerical analysis model of H-beam, where k_u: the horizontal spring rigidity, k_β: the rotational spring rigidity, l': the bracing interval, and $\overline{K}_f$: the fork rigidity. ABAQUS 2021 [4] was utilized for numerical analysis. H-beams are modelled with four-node shell elements, continuous braces with horizontal and rotational spring elements, and fork restraints at beam ends with rotational spring elements. The warping of beam end flanges is fixed, and the boundary condition is pin–pin roller. Continuous braces are assumed to be rigidly connected to the upper flange. As shown in Fig. 4, the bending moment at the beam end is converted to an axial force based on the dominant area proportion at each node. Eigenvalue analysis is conducted using this model, and the validity of the equations is confirmed by comparing them with the elastic lateral buckling load equations from Section 3 and beyond.

3 ELASTIC LATERAL BUCKLING LOAD FOR CONTINUOUSLY BRACED H-SHAPED BEAMS WITH FORK RESTRAINT

This section derives the elastic lateral buckling load equation for a continuously braced H-beam with fork restraint under a gradient bending moment. The potential energy U for this calculation, assuming fully fixed support, is given in eqn (3).

$$U = \frac{1}{2}\int_0^l \left\{EI_f u''^2 + E\Gamma\beta''^2 + GK\beta'^2 + k_u {u_1}^2 + k_\beta \beta^2 \pm \left(P_{11} - \frac{P_{11}-P_{12}}{l}x\right){u_1}'^2 \pm \left(P_{21} - \frac{P_{21}-P_{22}}{l}x\right){u_2}'^2\right\} dx. \quad (3)$$

where EI_y: the flexural rigidity about the weak axis, $E\Gamma$: the bending torsional rigidity, GK: the torsional rigidity, u: the average horizontal deformation of the upper and lower flanges (u_1 and u_2) and β: the torsional deformation. The deformations u and β are calculated using eqns (4) and (5).

$$u = (u_1 + u_2)/2. \quad (4)$$

$$\beta = (u_1 - u_2)/d. \quad (5)$$

It is assumed that u during lateral buckling is a trigonometric function as shown in eqn (6). In this paper, β is omitted because the undefined coefficients are set as b_1 to b_n instead of a_1 to a_n, following the same form as eqn (6).

$$u = a_1 \sin^2\frac{n\pi}{l}x + \cdots + a_n \begin{cases} \sin^2\frac{10n\pi}{13l}x. & \left(0 \le x \le \frac{13l}{20n}\right) \\ \sin\left(-\frac{10n\pi}{7l}x + \frac{10\pi}{7}\right). & \left(\frac{13l}{20n} \le x \le \frac{l}{n}\right) \\ (-1)^n \sin\left(-\frac{n\pi}{l}x - n\pi\right). & \left(\frac{l}{n} \le x \le \frac{(n-1)l}{n}\right) \\ (-1)^{n-1}\sin\left(\frac{10n\pi}{7l}x - \frac{10\pi}{7}\right). & \left(\frac{(n-1)l}{n} \le x \le \frac{(20n-13)l}{20n}\right) \\ (-1)^{n-1}\sin^2\left(-\frac{10n\pi}{13l}x + \frac{10n\pi}{13}\right). & \left(\frac{(20n-13)l}{20n} \le x \le n\right) \end{cases} \quad (6)$$

where n: the lateral buckling mode. By substituting u and β from eqn (6) into eqn (3) and performing partial differentiation, the elastic lateral buckling load P_{cr} is derived as shown in eqn (7).

$$\begin{bmatrix} A & 0 & B & C \\ 0 & D & C & E \\ B & C & F & 0 \\ C & E & 0 & G \end{bmatrix} \begin{Bmatrix} a_1 \\ a_2 \\ b_1 \\ b_2 \end{Bmatrix} = 0. \quad (7)$$

$$A=8J+\frac{3L}{4} \qquad C=H(1+m)P_{cr}d \qquad B=-\frac{O}{2}+\frac{3dL}{8} \qquad D=IJ+\frac{67L}{80}.$$

$$E=-\frac{2000}{91}+\frac{67dL}{160} \qquad F=2d^2J+GK+\frac{3d^2L}{16}+\frac{3M}{4} \qquad L=k_u\left(\frac{l}{\pi}\right)^2 \qquad I=\left\{\left(\frac{40}{13}\right)^3+2\left(\frac{20}{7}\right)^3\right\}$$

$$J=EI_f\left(\frac{\pi}{l}\right)^2 \qquad G=\frac{Id^2J}{4}+\frac{200GK}{91}+\frac{67L}{320}+\frac{67M}{80} \qquad M=k_\beta\tau_1\left(\frac{l}{\pi}\right)^2 \qquad O=(1-m)P_{cr}d$$

$$H=\frac{40}{13}\left[-\frac{13}{66}\sin\left(\frac{7\pi}{20}\right)+\left\{\left(\frac{13}{14}\right)^2-\left(\frac{13}{66}\right)^2\right\}\left\{\cos\left(\frac{7\pi}{20}\right)-1\right\}\right]-\frac{40}{7}\cos\left(\frac{3\pi}{20}\right)\left[-\frac{49}{204}+\left\{\left(\frac{7}{6}\right)^2-\left(\frac{7}{34}\right)^2\right\}\right].$$

Fig. 6 shows the relationship between elastic lateral buckling stress σ_{cr} and bending moment gradient m_B for a narrow H-beam H-500×250×9×16 with a slenderness ratio λ_1 = 280 under Type B. The boundary conditions of beam ends are warping-fixed (grey line) and fully fixed support (black line).

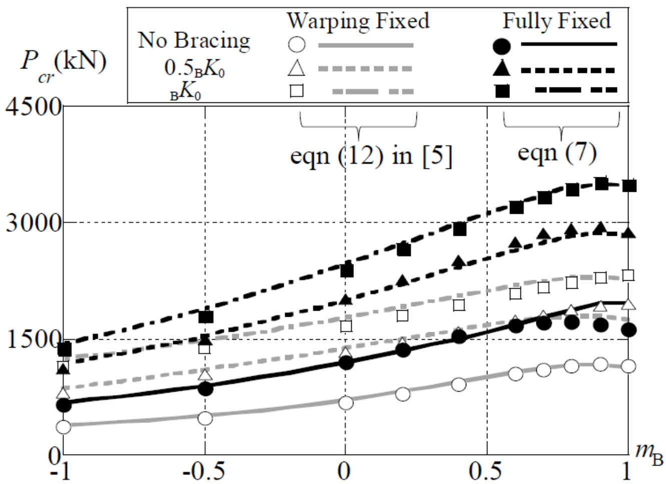

Figure 6: Relations between elastic lateral buckling load and moment gradient.

The elastic buckling load for warping-fixed support is eqn (12) in Kimura and Miya [5], and for fully fixed support, it is eqn (7). The parameter is bracing rigidity: no bracing (solid line), 0.5_BK_0 (dashed line), and $_BK_0$ (single point dashed line). Fully fixed support yields a higher lateral buckling load than warping-fixed support due to greater rigidity at beam ends. A larger bending moment gradient increases the lateral buckling load, as the beam deformation approaches the 2nd mode, reducing deformability. The plot shows numerical analysis results, and the derived equation generally reflects the relationship between elastic lateral buckling load and bending moment gradient.

However, eqn (7) is an 8×8 matrix and cannot express the elastic buckling load in an explicit form. Therefore, an approximate expression for eqn (7) is developed by functionalizing the effects of moment gradient and bracing rigidity from the matrix equation, and an elastic lateral buckling load equation is proposed for the case of fork restraint.

According to the Japanese design code [6], the lateral buckling load for a gradient bending moment is calculated by multiplying the lateral buckling load for a uniform bending moment by the moment modification factor C_1 (eqn (8)). The Japanese design code [6] pertains to simple support, non-braced H-beams. From Kimura and Sato [1], the elastic lateral buckling load equation for a continuously braced H-beam with warping and fully fixed support under uniform bending moments is given by eqns (9) and (10).

$$C_1 = 1.75 + 1.05m + 0.3m^2 \le 2.3. \tag{8}$$

$${}_kP_{cr2,m=-1} = \pm\frac{k_u}{2}\left(\frac{l}{n\pi}\right)^2 + \sqrt{\left\{\frac{k_u}{2}\left(\frac{l}{n\pi}\right)^2\right\}^2 + \frac{2(n^2-5n+15)}{5}\left[\frac{EI_f}{2}\left(\frac{n\pi}{l}\right)^2\left\{\frac{5-n}{2}EI_f\left(\frac{n\pi}{l}\right)^2 + \frac{GK}{d^2} - \frac{n-6}{5}k_u\left(\frac{l}{n\pi}\right)^2 + \frac{n+6}{10}\frac{k_\beta}{d^2}\left(\frac{l}{n\pi}\right)^2\tau_1\right\} + \frac{k_u}{4}\left(\frac{l}{n\pi}\right)^2\left\{\frac{GK}{d^2} + \frac{n+6}{10}\frac{k_\beta}{d^2}\left(\frac{l}{n\pi}\right)^2\tau_1 + \frac{n+5}{500}k_u\left(\frac{l}{n\pi}\right)^2\right\}\right]}. \tag{9}$$

$${}_kP_{cr3,m=-1} = \pm\frac{Bk_u}{4}\left(\frac{l}{n\pi}\right)^2 + \sqrt{\left\{\frac{Bk_u}{4}\left(\frac{l}{n\pi}\right)^2\right\}^2 + AEI_f\left(\frac{n\pi}{l}\right)^2\left\{\frac{A}{2}EI_f\left(\frac{n\pi}{l}\right)^2 + \frac{GK}{d^2} + B\frac{k_\beta}{d^2}\left(\frac{l}{n\pi}\right)^2\tau_1 + \frac{k_u}{2}\left(\frac{l}{n\pi}\right)^2\right\} + Bk_u\left(\frac{l}{n\pi}\right)^2\left\{\frac{GK}{d^2} + B\frac{k_\beta}{d^2}\left(\frac{l}{n\pi}\right)^2\tau_1\right\}}.$$

$$A = -0.36n + 2.9.,\ B = 0.07n + 0.6. \tag{10}$$

Here ${}_kP_{cr2,\,m=-1}$ and ${}_kP_{cr3,\,m=-1}$ represent the elastic lateral buckling load equations for warping and fully fixed support under uniform bending moments. The moment modification factor C_N is the ratio of the increase in lateral buckling load under any gradient bending moment to the lateral buckling load under a uniform bending moment. The right subscript N indicates 1: simple support, 2: warping-fixed support, and 3: fully fixed support.

Fig. 7(a) shows the relationship between the increase ratio of elastic lateral buckling load and moment gradient for a non-braced H-beam, with each boundary condition. The target cross sections are H-390×300×10×16, H-500×250×9×16, H-600×200×11×17, and the target slenderness ratios are λ_1=200, 240, 280. The vertical axis represents the ratio of elastic lateral buckling load at any bending moment gradient to that at a uniform bending moment, while the horizontal axis shows the bending moment gradient m ($-1 \le m \le 1$). Grey and black dotted lines correspond to eqn (12) in Kimura and Miya [5] and eqn (7), respectively, with plots showing numerical analysis results. The increase ratio in lateral buckling load is relatively insensitive to beam cross section and slenderness ratio. The equations align well with numerical analysis results. In the Japanese design code [6], the moment modification factor C_1 for simple support is given by eqn (8) and shown as a black line in Fig. 7(a).

The reduction in the increase ratio as the antisymmetric moment is approached, capped at 2.3 in the code. Fig. 7(a) indicates that the increase ratio for fully fixed support is similar to that for simple support, but greater for warping-fixed support compared to simple support.

Fig. 8 presents the deformation diagrams of upper and lower flanges during lateral buckling for each boundary condition. With warping-fixed support, rotational deformation occurs at the left end of the upper flange, where the compressive force acts, causing the lower flange to buckle in the same direction, linked to the upper flange. This phenomenon also occurs at the right end in the opposite direction, reversing the rotational deformation at both ends. This mutual constraint between flanges results in a greater increase ratio of elastic lateral buckling load compared to simple support. However, in the fully fixed support, as in the simple support, the upper and lower flanges do not affect each other's deformation at beam end, so the increase ratio of elastic lateral buckling load is equal.

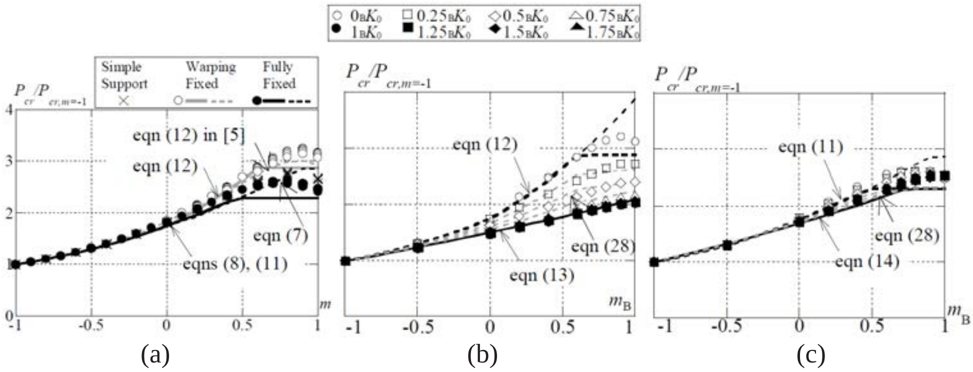

Figure 7: Relations between ratio of lateral elastic buckling load and gradient flexural moment (Type B). (a) No bracing; (b) Warping fixed support; and (c) Fully fixed support.

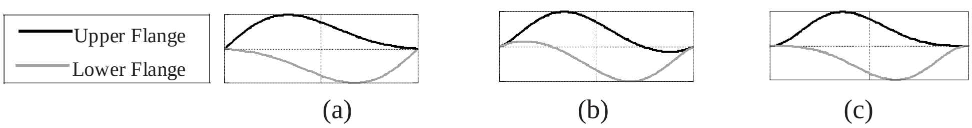

Figure 8: The deformation diagrams of upper and lower flanges during lateral buckling (m = 1). (a) Simple support; (b) Warping fixed support; and (c) Fully fixed support.

From the above, the moment modification factor C_3 for fully fixed support is assumed to be the same as that for simple support, as shown in eqn (11).

$$C_3 = C_1. \tag{11}$$

The moment modification factor C_2 for warping-fixed support is proposed as shown in eqn (12) from Kimura and Miya [5], based on the numerical analysis results in Fig. 7(a).

$$C_2 = \begin{cases} C_1. & (m \leq 0) \\ C_1(1 + 0.25m) \leq 2.875. & (0 \leq m) \end{cases} \tag{12}$$

Thus, the moment modification factor C_N was defined for the non-braced case.

Next, the moment modification factor with continuous bracing is discussed. Figs 7(b) and 7(c) show the relationship between the increase ratio in lateral buckling load and the bending moment gradient, considering bracing rigidity. Fig. 7(b) represents warping-fixed support, and Fig. 7(c) represents fully fixed support. White plots indicate rigidity below the reference required rigidity ratio ${}_{\mathrm{B}}K_0$, while black plots indicate rigidity above it. The upper limit of the increase ratio for no bracing is plotted and defined by eqn (12) for warping-fixed support and eqn (11) for fully fixed support. Black plots above ${}_{\mathrm{B}}K_0$ show that the increase ratio is constant, representing the lower limit of the increase ratio. The lower limit of the moment modification factor for warping-fixed support is defined in Kimura and Miya [5] as shown in eqn (13).

$$C_2{}' = C_1{}'(0.1m + 1.1). \tag{13}$$

In this paper, we propose eqn (14) as the lower limit of the moment modification factor for fully fixed support, corresponding to the lower limit of the black plot in Fig. 7(c).

$$C_3{}' = C_1{}'(0.23m + 1.23) \leq 2.3. \tag{14}$$

From the above, the moment modification factor was defined for cases exceeding ${}_kK_0$, and the lower limit of the rigidity modification factor was established.

Next, the moment modification factor is examined for cases where the rigidity ratio is less than or equal to ${}_kK_0$. As shown in Figs 7(b) and 7(c), the moment modification factor C_N for no bracing is the upper limit, C_N' above ${}_\mathrm{B}K_0$ is the lower limit, and factors below ${}_\mathrm{B}K_0$ are distributed between them for each bracing rigidity. We define the ratio of change in the moment modification factor, varying with bracing rigidity below ${}_kK_0$, as the bracing modification factor ${}_k\gamma_{a,b,N}$. Here, the left subscript k denotes A: Type A or B: Type B, and the right subscript N indicates 1: simple support, 2: warping-fixed support, and 3: fully fixed support. a is the ratio of the horizontal rigidity ratio $K_u/(EI_f/l^3)$ to ${}_kK_0$ in Fig. 4, and b is the ratio of the rotational rigidity ratio $K_\beta/(GK_f/d)$ to ${}_kK_0$. As shown in eqn (3), since braces are replaced by horizontal and rotational rigidity in this paper, ${}_k\gamma_{a,b,N}$, which vary with the rigidity, are expressed as a function of a and b.

Fig. 9(a) presents the bracing modification factors for Type A with fully fixed support, organized by horizontal rigidity ratio a, while Fig. 9(b) shows them organized by rotational rigidity ratio b. The vertical axis in Fig. 9 represents the bracing modification factor ${}_\mathrm{A}\gamma_{a,b,3}$. White plots indicate numerical results below ${}_\mathrm{A}K_0$, and black plots indicate results above ${}_\mathrm{A}K_0$. The numerical results are calculated by dividing the lateral buckling load $P_{cr,K}$ at any bracing rigidity by ($P_{cr,K0}$–$P_{cr,0}$), the difference between the lateral buckling load at ${}_\mathrm{A}K_0$ and with no bracing. The right subscript of P_{cr} denotes the rigidity level: 0 for no bracing, ${}_\mathrm{A}K_0$ for the reference required rigidity ratio, and K for any rigidity ratio. The lines in Fig. 9(a) correspond to b values from 0 to 1.75. The point (1,0) indicates a = 1 and b = 1, representing ${}_\mathrm{A}K_0$.

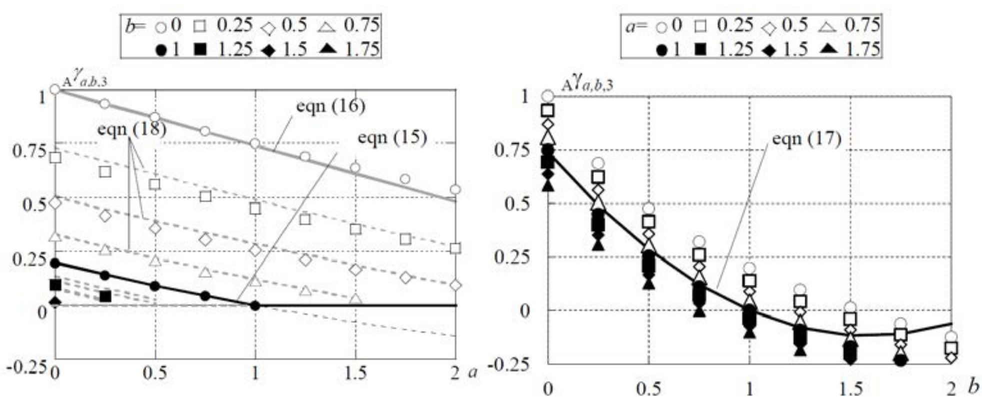

(a) (b)

Figure 9: Relations between moment correction factor and reference required rigidity ratio (Type A). (a) Lateral rigidity; and (b) Rotational rigidity.

From Fig. 9(a), for any a, the lower limit of the bracing modification factor ${}_{A}\gamma_{a,b,3}$ is represented by ${}_{A}\gamma_{a,1,3}$ (eqn (15)), approximated from numerical results for b=1 through the reference required bracing ratio (1,0). The upper limit of the bracing modification factor ${}_{A}\gamma_{a,b,3}$ is represented by ${}_{A}\gamma_{a,0,3}$ (eqn (16)), approximated from numerical results for b=0 through no bracing (0,1).

$$ {}_{A}\gamma_{a,1,3} = 0.03a^2 - 0.23a + 0.2. \tag{15}$$

$$ {}_{A}\gamma_{a,0,3} = 1 - 0.26a. \tag{16}$$

Then, as shown in Fig. 9(b), the ratio of change in the bracing modification factor (eqn (17)) at a = 1 is expressed by b. Eqns (15) and (16), which define the upper and lower bounds of the bracing modification factor ${}_{A}\gamma_{a,b,3}$, are interpolated using eqn (17).

$$ {}_{A}\gamma_{1,b,3} = 0.34b^2 - 1.08b + 0.74. \tag{17}$$

From the above, the bracing modification factor ${}_{k}\gamma_{a,b,3}$ is derived as shown in eqn (18) using any combination of bracing rigidityes (ak_{u0}, $bk_{\beta 0}$).

$$ {}_{k}\gamma_{a,b,N} = {}_{k}\gamma_{a,1,N} + \frac{({}_{k}\gamma_{a,0,N} - {}_{k}\gamma_{a,1,N})({}_{k}\gamma_{1,b,N} - {}_{k}\gamma_{1,1,N})}{({}_{k}\gamma_{1,0,N} - {}_{k}\gamma_{1,1,N})}. \qquad \left(0 \le {}_{k}\gamma_{a,b,N} \le 1\right) \tag{18}$$

In addition, ${}_{k}\gamma_{a,b,N}$ is set to ${}_{k}\gamma_{a,b,3} \geq 0$ because ${}_{k}\gamma_{a,b,3} \geqq 0$ is the lower limit when the referenced required rigidity ratio is greater than or equal to the rigidity ratio. Eqn (18) is shown in Fig. 9(a) as a grey dashed line and aligns well with numerical results for any combination of a and b. The ${}_{k}\gamma_{a,1,N}$, ${}_{k}\gamma_{a,0,N}$, ${}_{k}\gamma_{1,b,N}$ for calculating the bracing modification factors ${}_{k}\gamma_{a,b,N}$ for other conditions were defined as in Fig. 9, by approximating the numerical results defined in eqns (19)–(27). For example, the bracing modification factor for Type A with warping-fixed support ${}_{A}\gamma_{a,b,2}$ can be calculated using eqns (19)–(21), for Type B with warping-fixed support ${}_{B}\gamma_{a,b,2}$ using eqns (22)–(24), and for Type B with fully fixed support ${}_{B}\gamma_{a,b,3}$ using eqns (25)–(27) in eqn (18).

$$ {}_{A}\gamma_{a,0,2} = 1 + 0.08a^2 - 0.53a. \tag{19}$$

$$ {}_{A}\gamma_{a,1,2} = 0.11a^2 - 0.52a + 0.41. \tag{20}$$

$$ {}_{A}\gamma_{1,b,2} = 0.17b^2 - 0.72b + 0.55. \tag{21}$$

$$ {}_{B}\gamma_{a,0,2} = 1 + 0.04a^2 - 0.2a. \tag{22}$$

$$ {}_{B}\gamma_{a,1,2} = 0.1a^2 - 0.38a + 0.28. \tag{23}$$

$$ {}_{B}\gamma_{1,b,2} = 0.39b^2 - 1.23b + 0.84. \tag{24}$$

$$ {}_{B}\gamma_{a,0,3} = 1 - 0.01a. \tag{25}$$

$$ {}_{B}\gamma_{a,1,3} = 0.013a^2 - 0.073a + 0.06. \tag{26}$$

$$ {}_{B}\gamma_{1,b,3} = \begin{cases} 0.71b^2 - 17b + 0.99. & (m \le 0) \\ -0.25b + 0.25. & (0 \le m) \end{cases} \tag{27}$$

From the above, we defined the ratio of change of the moment modification factor when bracing rigidity is less than or equal to ${}_kK_0$.

Next, the moment modification factor ${}_kC_N$" at any rigidity is calculated by interpolating between the moment modification factor at no bracing and the moment modification factor above ${}_kK_0$ as the upper limit, with ${}_k\gamma_{a,b,N}$ as the lower limit. In this case, ${}_kC_N$" is expressed by eqn (28).

$$ {}_kC_N{}'' = (C_N - C_N{}')_k\gamma_{a,b,N} + C_N'. \tag{28} $$

Eqns (12), (13) and (18) are used for warping-fixed support, while eqns (11), (14) and (18) are applied to eqn (28) for fully fixed support. Eqn (28) is depicted as a solid grey line in Figs 7(b) and 7(c). The numerical results generally align with this line, and the upper limits in eqns (11) and (12) are conservatively set.

Finally, in Kimura and Miya [5], the elastic buckling load equation ${}_kP_{crN}$ is proposed as eqn (29) for both warping-fixed and fully fixed support under gradient bending moment.

$$ {}_kP_{crN} = {}_kP_{crN,m=-1} \cdot C_N{}''. \tag{29} $$

Fig. 10 shows the relationship between elastic lateral buckling load and moment gradient for beams with fully fixed support. Eqn (7) is represented by a grey line, eqn (29) by a black line, and numerical analysis results by plots. The parameter is the rigidity of braces. The vertical axis shows the lateral buckling load P_{cr}, while the horizontal axis displays the bending moment gradient m_B for Type B in the upper row and m_A for Type A in the lower row. In eqn (29), Type B is depicted with a black dotted line and Type A with a solid black line, with the smaller value representing the elastic lateral buckling load.

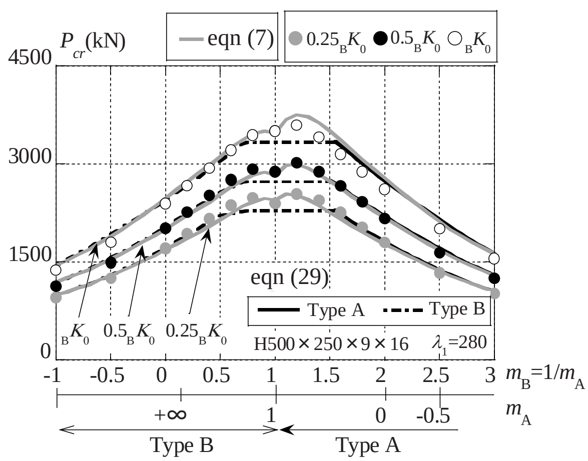

Figure 10: Relations between elastic lateral buckling load of gradient moment (fully fixed support).

The elastic lateral buckling load in eqn (7) aligns with numerical results, and eqn (31) provides a conservative evaluation of numerical analysis results.

These findings suggest that the lateral buckling load of an H-beam with fully fixed support can be assessed using eqn (29).

Table 1 presents the flow of the derivation process for the elastic lateral buckling load evaluation equation for continuously braced H-beams, considering the bending moment gradient.

Table 1: Induction flow of elastic lateral buckling load evaluation equation.

		Equations			
Lateral buckling load ($m = -1$)		${}_kP_{crN,m=-1}$			(9), (10)
Moment modification factor		${}_kC_N'' = (C_N - C_N')\,{}_k\gamma_{a,b,N} + C_N'$.			(28)
Upper and lower limit of moment modification factor		• C_N : No bracing • C_N' : More than K_0			(12), (11) (13), (14)
Lateral buckling load ($-1 \leq m \leq 1$)		${}_kP_{crN,m} = {}_kP_{crN,m=-1} \cdot {}_kC_N''$.			(29)
Ratio of change in ${}_kC_N''$ when $0<K<K_0$		${}_k\gamma_{a,b,N} = {}_k\gamma_{a,1,N} + ({}_k\gamma_{a,0,N} - {}_k\gamma_{a,1,N})({}_k\gamma_{1,b,N} - {}_k\gamma_{1,1,N})/({}_k\gamma_{1,0,N} - {}_k\gamma_{1,1,N})$.			(18)
		Type A (k = A)		Type B (k = B)	
Warping fixed support ($N = 2$)	${}_k\gamma_{a,0,N}$	$1+0.08a^2-0.53a$.	(19)	$1+0.04a^2-0.2a$.	(22)
	${}_k\gamma_{a,1,N}$	$0.11a^2-0.52a+0.41$.	(20)	$0.1a^2-0.38a+0.28$.	(23)
	${}_k\gamma_{1,b,N}$	$0.17b^2-0.72b+0.55$.	(21)	$0.39b^2-1.23b+0.84$.	(24)
Fully fixed support ($N = 3$)	${}_k\gamma_{a,0,N}$	$1-0.26a$.	(16)	$1-0.01a$.	(25)
	${}_k\gamma_{a,1,N}$	$0.03a^2-0.23a+0.2$.	(15)	$0.013a^2-0.073a+0.06$.	(26)
	${}_k\gamma_{1,b,N}$	$0.34b^2-1.08b+0.74$.	(17)	$m<0$: $0.71b^2-17b+0.99$. $m \geqq 0$: $-0.25b+0.25$.	(27)

An elastic lateral buckling load equation for continuously braced H-beams under ideal boundary conditions (warping-fixed and fully fixed support) is proposed. The elastic lateral buckling load ${}_kP_{cr4}$, when the fork deformation of beam ends is restrained, lies between the warping-fixed and fully fixed support and is proposed as shown in eqn (30):

$$ {}_kP_{cr4} = ({}_kP_{cr3} - {}_kP_{cr2})\overline{\tau_f} + {}_kP_{cr2}, \tag{30}$$

where, $\overline{\tau}_f$ is the ratio of fork restraint, with 0 representing free lateral bending (+fixed warp) and 1 representing fully fixed (fixed lateral bending + fixed warp), as shown in eqn (30). In Kimura and Sato [1], the fork restraint for H-beams under uniform bending moments is proposed as eqns (31)–(33). The τ_f in eqn (31) represents the ratio of fork restraint at the beam ends by the column, expressed in terms of the end rotational rigidity ratio s_f, which ranges from 1 to 4, as shown in eqn (32); s_f is the ratio of fork rigidity to the bending rigidity of the compression side flange, as shown in eqn (33). $\overline{K}_f$ is the fork rigidity in eqn (2). Numerical analysis confirms that eqns (31)–(33) can evaluate the ratio of fork restraint between warping-fixed and fully fixed support.

$$\overline{\tau_f} = (\tau_f - 1)/3. \tag{31}$$

$$\tau_f = 4 - 3/(1 + 2s_f). \tag{32}$$

$$s_f = (\overline{K_f}/l)/\left\{(\pi/l)^2 EI_f\sqrt{(C_2 + C_3)/2}\right\}. \tag{33}$$

Fig. 11 shows the relationship between the elastic lateral buckling load and the moment gradient when the fork deformation of beam ends is restrained. The beam cross-section is H-500×250×9×16, with λ_1 = 280. Fig. 11(a) shows no bracing, while Fig. 11(b) depicts continuous bracing ($0.5{}_BK_0$), with the parameter being the ratio of fork restraint. The black line represents eqn (30), the dashed grey line represents eqn (12) in Kimura and Miya [5] and eqn (7), and the plots show numerical analysis results. The numerical analysis results generally align with the proposed lateral buckling load equation for beams with fork restraints. These findings suggest that the elastic lateral buckling load can be evaluated using eqn (30).

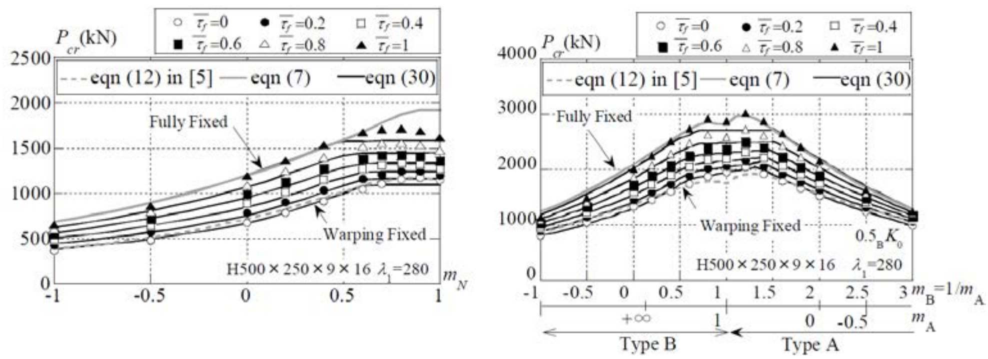

(a) (b)

Figure 11: Relations between elastic lateral buckling load and gradient of flexural moment (fork restraint). (a) No bracing; and (b) Continuous bracing 0.5BK0.

4 CONCLUSION

1. An elastic lateral buckling load equation for a continuously braced H-beam under a gradient bending moment with fully fixed support is derived using the energy method and its validity was confirmed.
2. The elastic buckling evaluation equation is proposed in an explicit form, considering the relationship between the terms of the lateral buckling load equation, and it was confirmed that the evaluation could be done on the safe side.
3. An elastic lateral buckling load equation with fork restraint is proposed and validated by interpolating the elastic lateral buckling loads of warping-fixed and fully fixed support.

REFERENCES

[1] Kimura, Y. & Sato, Y., Effect of warping restraint of beams to column joint on lateral buckling behavior for H-shaped beams with continuous braces under gradient flexural moment. *Journal of Structural and Construction Engineering*, **86**(779), pp. 145–155, 2021. https://doi.org/10.3130/aijs.86.145.
[2] Yoshino, Y., Liao, W. & Kimura, Y., Restraint effect on lateral buckling load of continuous braced H-shaped beams based on partial frame loading tests. *Journal of Structural and Construction Engineering*, **87**(797), pp. 634–645, 2022. https://doi.org/10.3130/aijs.87.634.
[3] JFE Steel Corporation, *Steel Structure Design Manual*, JFE Steel Corporation: Tokyo, 2022.
[4] Dassault Systèmes, ABAQUS/CAE 2021, Dassault Systèmes Simulia Corp.: Providence, RI, USA, 2021.
[5] Kimura, Y. & Miya, M., Effect of warping restraint of beams to column joint on lateral buckling behavior for H-shaped beams with continuous braces under gradient flexural moment. *Journal of Structural and Construction Engineering*, **84**(766), pp. 1601–1611, 2019. http://doi.org/10.3130/aijs.84.1601.
[6] Architectural Institute of Japan, Standard for Structural Calculation of Steel Structures, AIJ: Tokyo, 2005.